J Nanostruct 16(1): 603-616, Winter 2026

RESEARCH PAPER

Cytotoxicity, Anti-Multidrug-Resistant *Staphylococcus Aureus*, to Newly Green Synthesized, Copper Nanoparticles- Allium

Duaa Sameer khazaal *, Majid Rasheed Majeed

Department of Biotechnology, College of Science, University of Baghdad, Baghdad, Iraq

ARTICLE INFO

Article History:
Received 13 August 2025
Accepted 17 December 2025
Published 01 January 2026

Keywords:
Allium ampeloprasum
Antibacterial
Copper nanoparticles
Green synthesis

ABSTRACT

The resistance to the most antibiotics increasing has led to an urgent need to alternative treatments development. Nanotechnology is a young scientific field offers promising solutions because of its potent impact of therapeutic as an alternative to most conventional therapies. In this study, copper nanoparticles (CuNPs) were synthesized via eco-friendly green synthesis of using *Allium ampeloprasum* extract as a natural reducing and stabilizing agent. The synthesized CuNPs were thoroughly characterized using multiple techniques including, Fourier Transform Infrared Spectroscopy (FTIR), Ultraviolet-Visible Spectroscopy (UV-Visible), Field Emission Scanning Electron Microscopy (FE-SEM), X-ray Diffraction (XRD), Zeta Potential Analysis, Dynamic Light Scattering (DLS) and cytotoxicity test. The characterization confirmed the formation of pure, stable nanoparticles with size22.5 nm and 21.1 nm to 44 nm in width, with others around and a zeta potential of -22.3 mV, indicating good colloidal stability. The antibacterial activity of CuNPs was evaluated against multidrug-resistant (MDR) bacterial strains *Staphylococcus aureus*. The nanoparticles exhibited maximum inhibition activity across a concentration range of 1.9–1000 µg/ml, with the maximum inhibition zone reaching to 27.4, 27 and 21mm for *S. aureus* and without cytotoxic effect on the normal human dermal fibroblasts neonatal. These findings highlight the promising antibacterial efficacy and biocompatibility of green-synthesized CuNPs, supporting their potential application in biomedical and antimicrobial therapies.

How to cite this article
Sameer khazaal D., Rasheed Majeed M. Cytotoxicity, Anti-Multidrug-Resistant Staphylococcus Aureus, to Newly Green Synthesized, Copper Nanoparticles- Allium. J Nanostruct, 2026; 16(1):603-616. DOI: 10.22052/JNS.2026.01.054

INTRODUCTION

Nanoscience and nanotechnology are among the most scientific significant modern fields focusing on the study of the nanoscale matter, bridging the gap between materials bulk with atomic or molecular structures. At this scale, materials exhibit unique physical and chemical properties that fundamentally differ from their counterpart's bulk, due to their high surface-to-volume ratio and quantum effects primarily. These properties enable metallic nanoparticles to demonstrate mechanical, magnetic, distinctive electronic and chemical behaviors, which have wide applications in biosensing, medicine, electronics and catalysis [1-4]. Among metals, copper nanoparticles CuNPs have garnered increasing attention due to their remarkable physicochemical properties including thermal conductivity, excellent electrical, potent biological activity and cost-effectiveness [5]. CuNPs can be

* *Corresponding Author Email: doaa.samir2406p@sc.uobaghdad.edu.iq*

synthesized using chemical, physical and biological methods which have high efficiency though they consume a lot of energy. Although various physical and chemical methods exist to synthesize CuNPs, many suffer from environmental and health drawbacks due to the use of toxic chemicals and high energy consumption, also can cause a variety of chemicals use can cause serious environ mental issues in addition to these methods are not intensive and costly "Therefore, these methods are applied less widely in the industrial production. Therefore, biological methods have been emerged as an alternative method for the safe and nanoparticles sound synthesis. Consequently, green synthesis approaches, which utilize natural sources like plant extracts as reducing and stabilizing agents, have gained prominence. Plant extracts are rich in bioactive compounds—such as flavonoids, phenolic acids, tannins, and alkaloids—that facilitate the reduction of copper ions and stabilize the nanoparticles, while enhancing their antimicrobial properties. [6-7]. Copper is an essential trace element in living organisms, involved in vital processes such as wound healing, bone formation, angiogenesis and enzyme activation [8-10]. It also catalyzes the crosslinks formation in collagen and elastin precursors. Moreover, copper is essential for the normal physiological functions of microorganisms maintaining [11-13]. It also possesses antimicrobial properties that have been recognized since ancient times with low toxicity compared to silver relatively [14]. Multidrug-resistant (MDR) bacteria remain one of the greatest challenges in public healthcare, as the increasing resistance of pathogens to antimicrobial drugs complicates infection treatment despite advances in nanotechnology. Recent advances in nanotechnology offer promising opportunities for developing novel formulations using CuNPs have antimicrobial activity with different sizes, shapes, and antimicrobial properties, which act as carriers for antibiotics and natural antimicrobial compounds; the emergence of bacterial resistance to these nanoparticles remains a critical concern. However, the emergence of MDR against these nanomaterials is a significant challenge in antimicrobial nanotechnology, due to their ability to interact with bacterial cells at the nanoscale. However, recent studies show that bacteria can develop resistance mechanisms against these materials, potentially reducing their long-term effectiveness. [15-16]. Pervous studies have demonstrated that CuNPs effectively inhibit the growth of MDR bacteria such as *Staphylococcus aureus*, positioning them as potent alternatives for combating resistant infections. This study reports the biosynthesis of CuNPs using leek (*Allium ampeloprasum* L.) extract as a natural reducing and stabilizing agent. The antibacterial efficacy of these biosynthesized CuNPs was evaluated against multidrug-resistant bacteria, specifically *Staphylococcus aureus*. Comprehensive characterization of the synthesized nanoparticles was performed using UV-Vis spectroscopy, Fourier Transform Infrared Spectroscopy (FT-IR), Zeta Potential analysis, Field Emission Scanning Electron Microscopy (FE-SEM), Dynamic Light Scattering (DLS), and X-ray Diffraction (XRD).

MATERIALS AND METHODS

Collection and culturing of the clinical specimens

Fifty one of *S. aureus* were collected from patients at the Burn Center of Medical City Hospitals (Baghdad) between February 1, 2024 and November 20, 2024 for pathogenic bacterial isolation. Using cotton swabs to obtained from burns specimens and accompanied by patient data (age, gender, and sample source). The samples were initially cultivated in nutrient broth, which served as a transport medium, and then transported to the laboratory at the University of Baghdad. The cultures were incubated at 37°C for 24 hrs. Then the samples in order to isolate and identify the bacterial isolates were sub-cultured on to blood agar, mannitol salt agar, and incubated for another 24 hr. at 37°C upon the morphological characteristics [15-19]. Additionally, were confirmed the identifications through subculture on a combination of culture media biochemical tests and VITEK-2 systems.

Antibiotic Sensitivity Test

The method of Kirby-Bauer disc diffusion [20-21] was for conducting the antibiotic susceptibility test used according to the following procedure: first were prepared Muller Hinton agar plates according to the manufacturer's company instructions, and then poured into sterile Petri dishes each containing of the prepared medium25 ml. After that touch one colony of the bacterial culture and was added to 5 ml of sterile normal saline, and then mix it very well to achieve a concentration of 1.5 × 108 CFU/ml of culture adjusted to the 0.5 turbidity standard of

MacFarland. Were submerged sterile swabs in the inoculum and on the side of the tube compressed to discard any excess liquid and then on the agar plate surface rubbed three times at 60° to ensure even distribution. The selected antibiotics were added with sterile forceps to the inoculated surfaces, then incubated the plates at 37°C for 24 hr., and the inhibition zone diameter was measured with a metric ruler, as shown was using ten different antibiotic discs for each isolates. For *S. aureus*, the discs were used: penicillin, rifampin, azithromycin, linezolid, clindamycin, levofloxacin, ciprofloxacin, trimethoprim/sulfamethoxazole, gentamicin, and doxycycline. Were classified the isolates as sensitive (S), intermediate resistance (I), and resistant (R) according to the 2024 Clinical and Laboratory Standards Institute (CLSI) instructions [22].

Preparation of Allium ampeloprasum L.

Fresh leaves of *Allium ampeloprasum* were purchased from a vegetable market in Baghdad, Iraq. The leaves were washed with tap water and rinsed with deionized distilled water (DDW) to remove dust particles. After washing, the extract was prepared by crushing 100 g of the leaves and mixing them with 400 mL of deionized water in a 500 mL conical flask (at a s:l ratio of 1:4), then heating the mixture at 70 °C using a heater-stirrer for approximately 18 minutes. After that, the crude extract was allowed to cool and was filtered using Whatman No. 1 filter paper. The filtrate was then further centrifuged at 3500 rpm for 20 minutes to remove any remaining debris. This method was described by [23] with modifications including adjusting the boiling temperature to 70 °C and centrifugation at 3500 rpm for 20 minutes instead of the original conditions described in the reference. These modifications were made to optimize the extraction process and improve the clarity and stability of the final extract shown in Fig. 1.

Biosynthesis of copper nanoparticles

Cupric chloride anhydrous ($CuCl_2$, 98%) was purchased from (Sigma/USA) for the synthesis of copper nanoparticles (CuNPs). Ten grams of $CuCl_2$ were dissolved in 100 mL of double-distilled water with continuous stirring using a magnetic stirrer. Subsequently, 250 mL of *A. ampeloprasum* extract was added dropwise to the copper chloride solution while maintaining stirring at room temperature. Upon interaction, the reaction mixture was left for 24 hours to allow complete contact with chloride ions. During this period, the color of the solution spontaneously changed from bluish to dark greenish to homogeneous reddish-brown suspended particles, indicating the formation of copper nanoparticles. The resulting mixture was centrifuged at 3500 rpm for 20 minutes. After decantation, the presence of CuNPs was confirmed. These particles were washed three times with deionized water to remove debris and then dried in an incubator at 37 °C for three days; this method was adapted with modifications from [24].

Characterization of Biosynthesized CuNPs
UV-Vis Spectroscopy of the CuNPs

The ultraviolet-visible (UV-Visible) spectrophotometer was used to the nanoparticles determine optical properties, which has 1 nm resolution, 2 ml utilizing quartz cuvette with a 1 cm optical path length. Firstly, were in DDW suspended CuNPs by placing it in a sonicator bath for 15 min. to the facilitate measurement with a

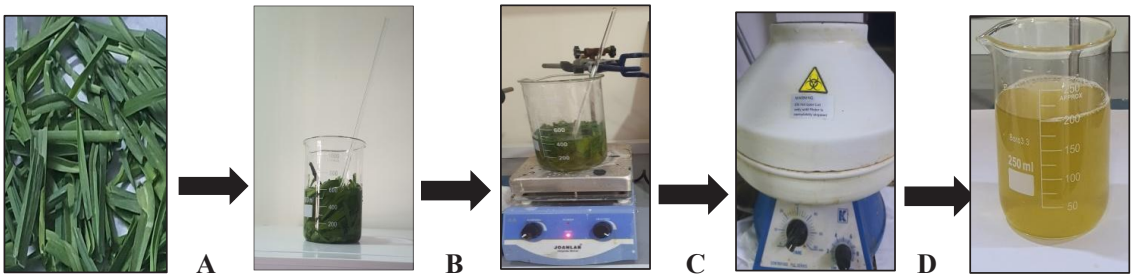

Fig. 1. Prepration of *Allium ampeloprasum* leaf extract (A) leaves washed and crushed (B) Leaves boiled at 70 °C for about 18 minutes in 400ml double-distilled water (C) Centrifuged for 20 min at 3500 rpm to remove biomaterials (D) Filtered with Whattman filter paper No. 1 to remove solid particles.

spectrophotometer. The DDW was used as the blank reference in order to the spectrophotometer calibrate. Was determined the optimal scanning range for the samples between 500 nm and 1100 nm, with a scanning speed of 500 nm/min. were conducted the measurements in the Chemistry Department, College of Science, University of Baghdad, Iraq[25].

Fourier Transform Infrared Spectroscopy (FT-IR)

The FTIR spectrum was obtained using (Shimadzu 8400) FTIR spectrometer. A minute quantity of them in addition to dried nanoparticle was mixed separately with potassium bromide and into individual pellets each was formed using a special machine, then with an FTIR device measured. Additionally, glass slides of plant extract were prepared and allowed to dry, also to characterize with FT-IR. The spectra were recorded within the range of 4000 cm^{-1} to 400 cm^{-1} wave numbers to identify the different functional groups [26-27]. The experiment was conducted at the University of Baghdad, College of Science, Department of Chemistry.

Field Emission Scanning Electron Microscopy (FE-SEM)

Uses a focused beam of high-energy electrons to scan the surface of a sample, producing high-resolution images of morphology and surface structure and diameter have been characterized with FE-SEM. The CuNPs dried samples were positioned on a glass slide, followed by the platinum coating application to their electronic conductivity enhance [28].This test was performed in the Fullerene Center.

X-ray Diffraction (XRD)

The diffractometer of X-ray used to the X-ray diffraction spectrum record to the synthesis of the nanoparticles verify and the crystalline structure of the biosynthesized CuNPs identifies. This test was performed in the Fullerene Center [29].

Zeta Potential Analysis

The CuNPs zeta potential of was estimated using a zeta seizer to determine their colloidal dispersion stability. The tests of the CuNPs zeta potential were carried out at 25 °C using a disposable foldable capillary cell with electrodes and distilled water as a dispersant. Were calculated the results as the average of ten measurements taken in a run [30].

Dynamic Light Scattering (DLS)

The system particle sizing of nanoparticles measures by analyzing the fluctuations in scattered light caused by the Brownian motion of the particles also was used to determine the size distribution for Cu solution was carried out at [31].

Cytotoxicity Assay of CuNPs

To the cell viability of various CuNPS concentrations evaluate at (1000, 500, 250, 125, 62.5, 31.25 and 15.62 µg/ml), as reported previously, the MTT test against on the normal human dermal fibroblasts neonatal (HdFn cells) was utilized. The viability of cells percent exposed to treatments was calculated using the following equation and the concentration that inhibits 50% of cell growth was used as a for cytotoxicity [32] parameter: Cell Viability (%) = (Mean OD of Treated Cells/Mean OD of Control Cells) × 100.

Testing the antibacterial activity of CuNPs

The antibacterial activity of CuNPs was used to evaluate against Gram-positive *S. aureus.* The method of agar well diffusion was performed according to the following procedure [33]: The agar of Muller Hinton was prepared according to the manufacturer company instructions and poured into sterilized Petri dishes then left to solidify. The inoculums have been produced by putting of single colony touch into a 5 ml tube of normal saline to concentration of 1.5 x 108 cell/ml achieve and equivalent to the 0.5 McFarland turbidity standard. The plates by immersing a sterile swab were inoculated in the inoculum. The wells of agar were made with a sterilized corkborer. The suspending solutions were made from (1.95- 1000 µg/ml). The solutions in the sonicator bath were placed for 15 min. A sterile corkborer was used to create five wells of 6 mm diameter in each plate were then filled with 100 µl of varied concentrations from (1.95 - 1000 µg/ml) were into the poured and labelled wells in plates at 37°C for 24 hrs. Were incubated after the incubation period, the antibacterial efficacy of CuNPs was determined by the inhibition zones diameter measuring with a millimeter ruler.

Determination of minimum inhibition Concentration (MIC) of CuNPs

The antibacterial activity of CuNPs was evaluated against *S. aureus* using the microdilution method [34]. Each isolates of *S. aureus* was inoculated into

in medium of Mueller-Hinton Broth (MHB) and cultured at 37°C for 24 hrs, the stock solution of CuNPS (1000µg/ml) was diluted to produce two-fold serial dilutions ranging from 1.95 µg/ml to 1000 µg/ml. Were transferred CuNPS dilutions to microplate wells and then inoculated with a bacterial sample with a turbidity of 0.5 McFarland standard. Was used MHB Medium as a negative control, while used bacterial suspension without any addition was as a positive control for 24 hours, was incubated the microplate at 37°C. Then, in each well, were examined bacterial growth and the minimum concentration of the prevented noticeable growth, was considered as MIC [22].

The Statistical analysis

GraphPad Prism 9.2 was used to the statistical analysis conduct to evaluate the impact of various types of nanoparticles and their concentrations on S.aureus. When the p-value was less than 0.05, the differences were deemed significant. Differences among groups were assessed using the Kruskal–Wallis test followed by Dunn's multiple comparisons test. Data are presented as median and interquartile range (IQR) [35].

RESULTS AND DISCUSSION

Isolation of S. aureus

In this study, one hundred and fifty clinical burn samples (swabs) were collected from patients to examined, fifty isolates were identified as *S. aureus*. The characteristic of *S. aureus* colonies golden-yellow pigment, shiny, spherical, large in size with regular smooth, convex and opaque edges on maintol satl agar and other media [36] in Fig. 2.

Antibiotic Susceptibility Test

According to the findings shown in Fig. 3, all isolates displayed a high level of resistance (100%) to penicillin, followed by 72.0% resistance to rifampin and 34.0% to azithromycin. Lower

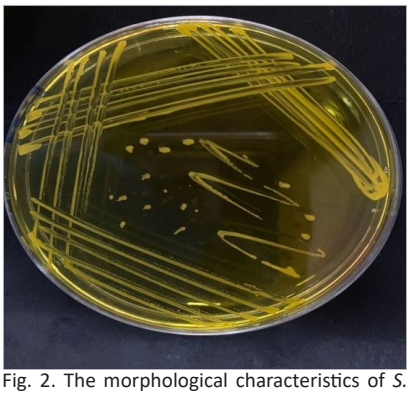

Fig. 2. The morphological characteristics of *S. aureus* on Mannitol salt agar.

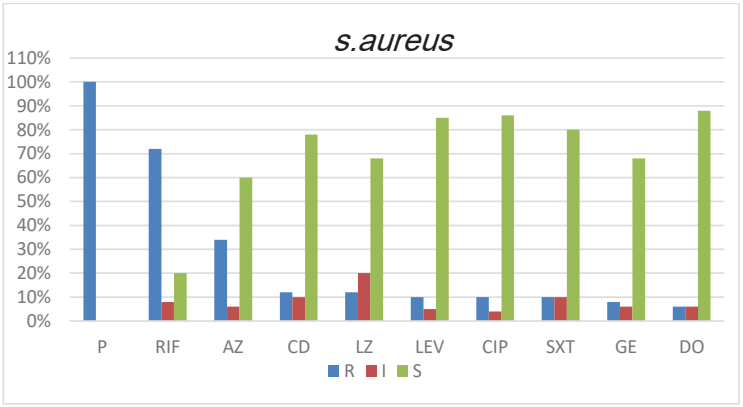

Fig. 3. Antibiotic susceptibility test of *S. aureus*.

resistance rates were observed for linezolid and clindamycin (12%), levofloxacin, ciprofloxacin, and trimethoprim/sulfamethoxazole (10% each), and gentamicin (8%). The lowest resistance among the tested antibiotics was recorded for doxycycline (6%). The current results reveal that 100% of *S. aureus* isolates were resistant to penicillin, indicating a widespread prevalence of penicillin-resistant strains. This finding agrees with a previous study conducted in Kabul, Afghanistan [37], which reported that 99% of *S. aureus* isolates exhibited high resistance to penicillin. That study also documented varying resistance levels to other antibiotics, including erythromycin (60%), gentamicin (16.2%), clindamycin (4.8%), trimethoprim–sulfamethoxazole (34.3%), and doxycycline (13.3%). A local study in Iraq [38] similarly reported that more than 90% of *S. aureus* isolates identified as methicillin-resistant (MRSA) from various clinical sources exhibited resistance to penicillin. This underscores the markedly reduced effectiveness of penicillin in treating MRSA infections and highlights the ongoing challenge of antibiotic resistance in regional clinical settings.

Biosynthesis of CuNPs

CuNPs were biosynthesized from *A. ampeloprasum*, the color changes alight blue to greenish blue and after centrifugation the production of reddish brown precipitate were indicators of the formation of CuNPs was obtained in Fig. 4. In recent years, an obvious attention to synthesizes nanomaterials by using plant extract (mainly silver, zinc, gold and copper) with remarkable properties has been observed in order to develop antimicrobials activities with in vitro against pathogenic bacteria other than antibiotics. Synthesized nanoparticles via leek extract demonstrate enhanced antibacterial, antioxidant, and catalytic activities, attributed to

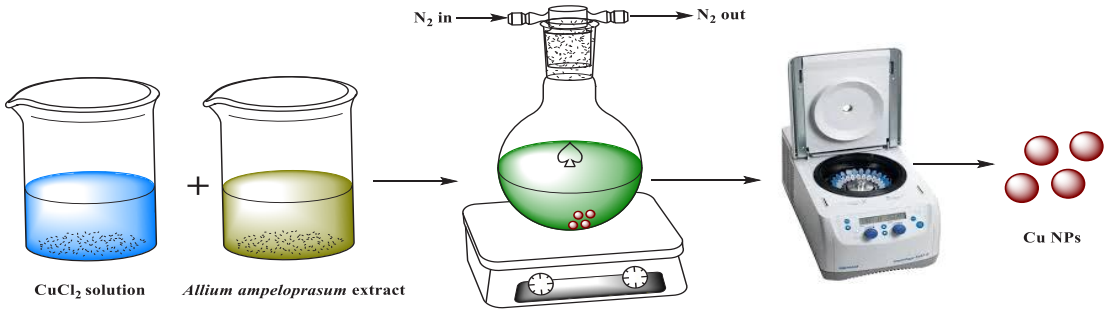

Fig. 4: steps of CuNPs preparation by biological methods.

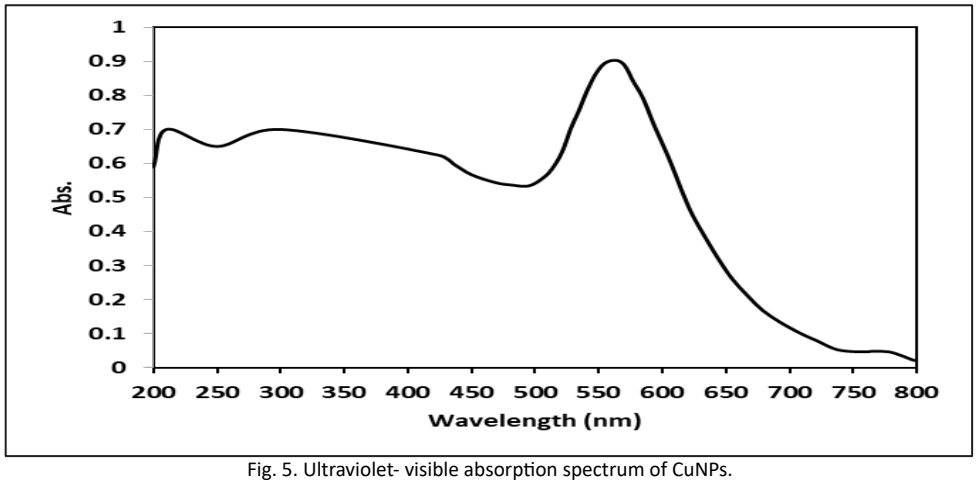

Fig. 5. Ultraviolet- visible absorption spectrum of CuNPs.

the synergistic effect of the metallic core and the bioactive phytochemical capping agents [39].

Characterization of CuNPs

UV–Vis Spectral Analysis

The biosynthesized CuNPs exhibited a strong absorption peak at approximately 557.8 nm, as shown in Fig. 5. However, presence of the plasmon resonance (SPR) band confirms the successful formation of metallic CuNPs peaks appear typically in the range of 560–600 nm depending on particle size and morphology. The results in agreement with the pervious study published by [40], indicated successfully formation of CuNPs using *Mentha longifolia* (mint) extract was peak appeared at 558 nm. Indicating of uniformly presence distributed and stable nanoparticles.

FTIR Analysis

The FTIR spectrum of the synthesized CuNPs was used to identify and approximate the biomolecules present in the *A. ampeloprasum* extract. Fig. 6 exhibited the FTIR spectrum characteristic peaks that can be directly correlated with the compounds identified by GC–MS. biosynthesis of copper nanoparticles. The broad band at 3292 cm^{-1} corresponds to O–H and N–H stretching vibrations, attributed to hydroxyl and amine groups derived from compounds such as Hexanedioic acid mono (2-ethylhexyl) ester and 3, 4, 4-trimethyl-1,2,6-oxadiazine N-oxide, indicating their role in the initial reduction and stabilization of the nanoparticles. The band at 3053 and 2960 cm^{-1} represent aliphatic and aromatic C–H stretching, which are consistent with the long alkyl chains of hexanedioic and decanedioic esters and the bicyclic ether structure, contributing to steric stabilization of the particles. Such hydrophobic chains are believed to provide steric hindrance, thereby preventing agglomeration and enhancing the colloidal stability of the nanoparticles, which agrees with similar findings in ester- and lipid-mediated nanoparticle stabilization. The absorptions at 1650 and 1641 cm^{-1} are assigned to C=O and C=C stretching, corresponding to dicarboxylic esters and aromatic groups in pyrimidine derivatives, suggesting the involvement of carbonyl groups. The band at 1539 cm^{-1} is attributed to Amide II or NO_2 vibrations, which are linked to nitrogenous compounds such as oxadiazine N-oxide and pyrimidine-nitro derivatives, highlighting their role in coordination and surface stabilization. Band at 1454 and 1398 cm^{-1} correspond to C–H bending vibrations of long-chain esters, whereas the absorption at 1238 cm^{-1} is associated with C–O–C and C–N stretching from dioxabicyclic ether and nitrogen-containing compounds. The band at 1070 cm^{-1} further confirms C–O stretching of ester moieties. Finally, the band at 873 and 665 cm^{-1} correspond to out-of-plane aromatic C–H bending in pyrimidine derivatives which likely contribute to nanoparticle capping. These functional groups are well known to act as electron donors in the reduction of metal ions, as previously reported in plant-mediated nanoparticle synthesis. The Cu NPs do not exhibit vibrationally active Cu–Cu bonds within the infrared (FTIR) region, no characteristic vibrational

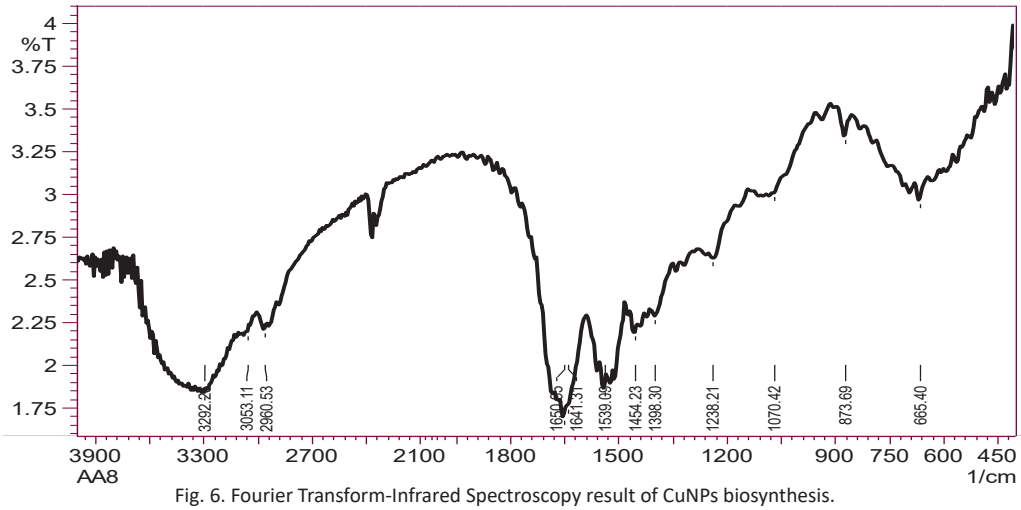

Fig. 6. Fourier Transform-Infrared Spectroscopy result of CuNPs biosynthesis.

bands are observed in the spectra. This is because Cu–Cu bond vibrations require higher energy than that provided by infrared photons, making them undetectable by FTIR spectroscopy. These results agree with the FTIR spectrum of biosynthesized CuNPs using *Marsilea quadrifolia* rhizome extract, which showed several absorption peaks indicating the presence of bioactive functional groups responsible for reduction and stabilization. A broad peak around 3292 cm^{-1} corresponds to O–H stretching of phenols and alcohols, while peaks at 3053 and 2960 cm^{-1} indicate aliphatic C–H stretching. Bands observed at 1650 and 1641 cm^{-1} are attributed to C=O and C=C vibrations, suggesting involvement of flavonoids or proteins. Additional peaks at 1539, 1454, 873, and 665 cm^{-1} confirm the presence of amide groups and aromatic compounds, which likely contribute to nanoparticle capping [41].

Field Emission Scanning Electron Microscope (FESEM)

FE-SEM images in Fig. 7 reveal that the sample comprises sheet /plate like particles together with smaller, almost spherical nanoparticles filling the interstices between the sheets. In the fine scale (200 nm) image, several sheets measure approximately 44 nm in width, with others around

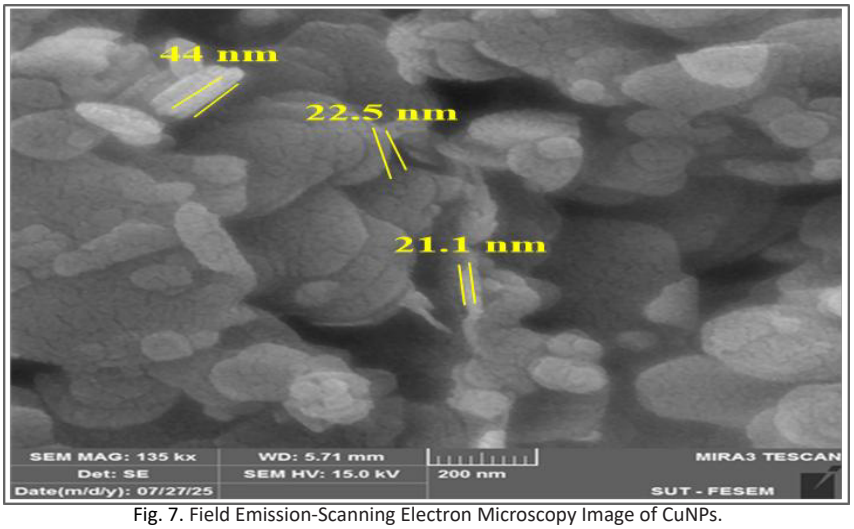

Fig. 7. Field Emission-Scanning Electron Microscopy Image of CuNPs.

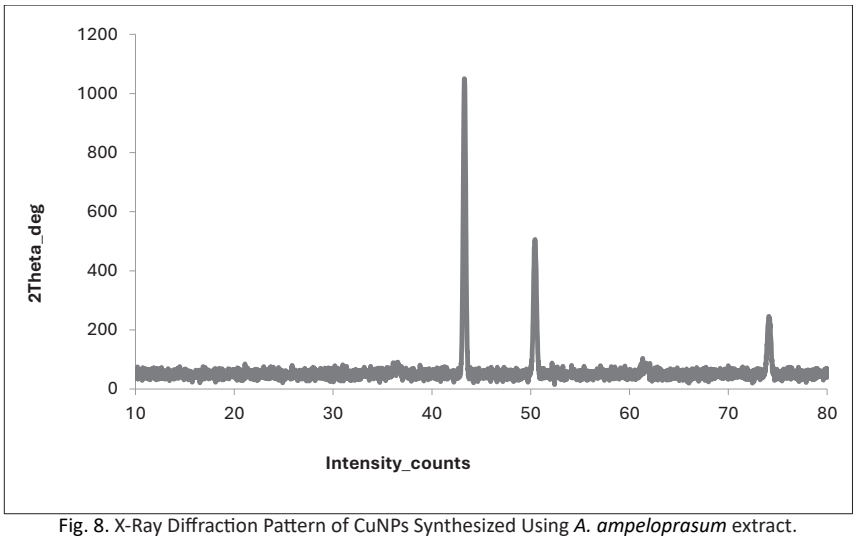

Fig. 8. X-Ray Diffraction Pattern of CuNPs Synthesized Using *A. ampeloprasum* extract.

22.5 nm and 21.1 nm. Plate like sheets extend laterally over larger areas, while smaller particles occupy spaces between them, illustrating a broad size distribution. The combination of varied sizes and plate like morphology, especially the presence of smaller sheets and sharp edges, increases local surface curvature. Edges and high curvature regions tend to host higher surface charge densities, which raises the energy barrier for electron emission from the surface in other words, the work function increases in those regions. Larger sheets contribute to extensive surface area while the smaller, sharply edged structures enhance curvature effects; together they push the overall work function upward. Accordingly, one can predict that the sample will manifest a relatively high work function, due to this synergy of large, expansive sheets and smaller, more curved edged particles. Such morphological and size features are particularly relevant for surface dependent applications, including catalysis, sensors, or optoelectronic devices. These results are in agreement with those reported by [42] where strong antibacterial activity using metallic copper nanoparticles of spherical shape and sizes between 20–60 nm. Although the study focused on spherical particles, the similarity in size supports the notion that smaller nanoparticles exhibit stronger antibacterial effects. However, the current sample's sheet-like structure, with higher curvature and more active edge sites, is expected to further enhance bacterial membrane interaction and increase antimicrobial efficiency.

X-ray Diffraction (XRD)

The XRD analysis of the biosynthesized (CuNPs) shown in Fig. 8 confirmed a face-centered cubic (FCC) crystalline structure characteristic of pure metallic copper. Sharp diffraction peaks were observed at 2θ values of 43.28°, 50.44°, and 74.10°, corresponding to the (111), (200), and (220) crystal planes, respectively, which match well with the standard JCPDS card no. 04-0836. The most intense peak at the (111) plane indicates a preferred crystallographic orientation. Crystallite sizes calculated using the Scherrer equation ranged from 22.37 to 29.12 nm, with an average size of approximately 25.5nm, the sharp peaks suggest high crystallinity and good structural quality [43], reflecting well-defined nanoclinic crystalline with high structural order.

Zeta potential

Zeta potential was used to a measure of the electrostatic charge of the CuNPs particles. The negative potential value was due to the presence of amino and carboxylic groups on the CuNPs surface were biologically produced were be -22.3 mV. Zeta potential is an important parameter that affects the stability of colloidal dispersion. Particles with high negative and or positive value than ±30 mV for zeta potential are usually considered to give rise to stable dispersions shown in Fig. 9 this result in agreement with the pervious study reported by

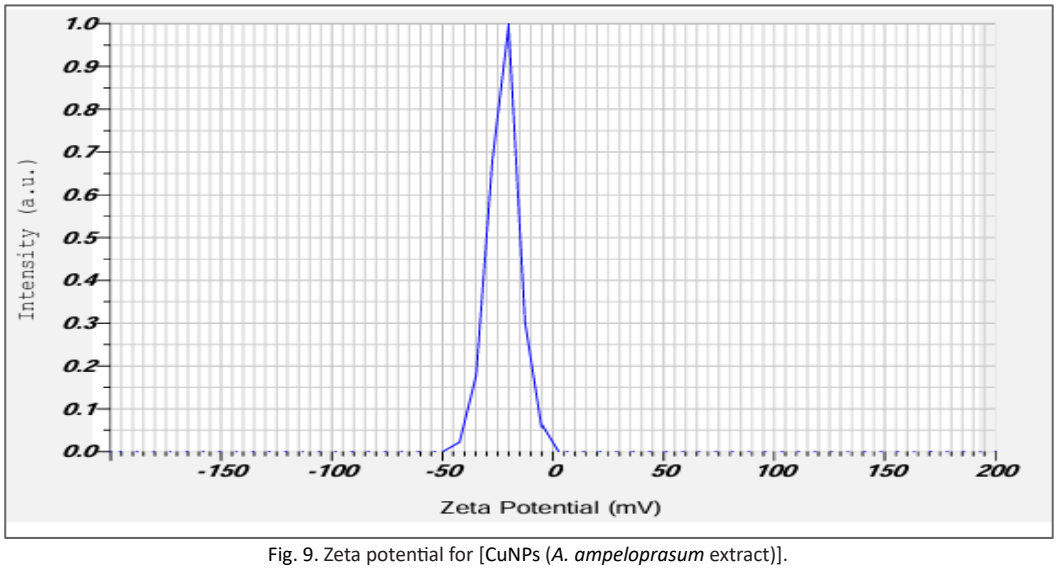

Fig. 9. Zeta potential for [CuNPs (*A. ampeloprasum* extract)].

[43] which is -22.47 mV.

Dynamic Light Scattering (DLS)

Tool is a very important for size of nanoparticles characterizing the in a solution. The DLS experiment showed that the CuNPs particle size of was 30.34 nm the study result shown in Fig. 10 is consistent with a previous study that supported by [44].

Cytotoxic Effect of CuNPs

The cytotoxic effect of CuNPs on the normal human dermal fibroblasts neonatal (HdFn) cell line was also investigated before and after treated with CuNPs shown in Fig. 11A, 11B. CuNPs is desirable to have antimicrobial efficacy while we carried out cytotoxicity studies of it on a model normal fibroblast cells (HdFn cells), without any reported clinical or pathological findings. "The dose-

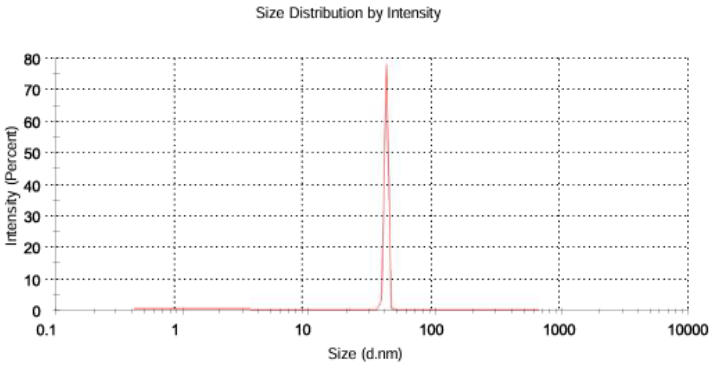

Fig. 10. Dynamic light scattering (DLS) images of CuNPs biosynthesis Using *A. ampeloprasum* extract.

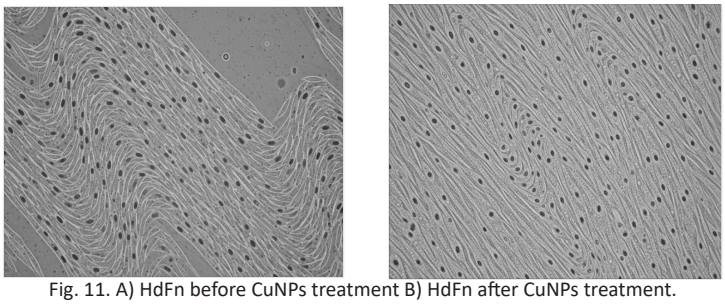

Fig. 11. A) HdFn before CuNPs treatment B) HdFn after CuNPs treatment.

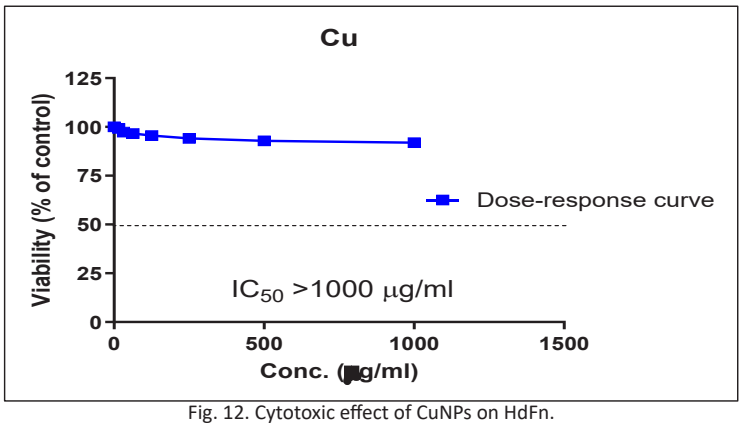

Fig. 12. Cytotoxic effect of CuNPs on HdFn.

response curve shows in Fig. 12 that viability of cells remain high even at concentrations of CuNPs up to approximately 1500 µg/ml, with viability staying above 90%. The IC50 value indicates that the concentration required to cell viability reduce by 50% is greater than 1000 µg/ml, suggesting that these nanoparticles relatively exhibit low toxicity within the tested concentration range." implying that the nanoparticles tested were safe and without noticeable adverse effects under the specific testing conditions. Making them suitable for applications involving direct interaction with cells, such as wound dressings or topical treatments, provided these concentration limits are not exceeded." The result of study disagreement by [45] indicated that the CuNP-coated fabric extracts exhibited significant toxicity to BJ cells, and cell viabilities (CVs) of 44.8 ± 11.1 and 21.2 ± 1.0% were determined for 10 µL and 30 µL samples respectively. The extracts of Cu–Ni NP-coated fabric exhibited much lower cytotoxicity, as evidenced by a higher average CV at 97.9 ± 9.9 and 50.0 ± 9.7% for 10 µL and 30 µL of extracts, respectively.

Antibacterial activity

The antibacterial activity of CuNPs results evaluate against *S. aureus* from the diameters of inhibition zones. Table 1 demonstrated that CuNPs possess antibacterial activity that depending on the bacterial isolate and the nanoparticle concentration. A direct correlation was observed between CuNP concentration and the diameter of the inhibition zone for all tested bacterial isolates. All three isolates of *S. aureus* isolates (*S.73, S.75* and *S.76*) showed clear susceptibility to CuNPs, especially at higher concentrations (1000 to 250 µg/ml)· The isolate *S.75* exhibited the highest sensitivity, maintaining a clear inhibition zone even at a low concentration of 7.8 µg/ml (12.9 mm in diameter) indicating strong susceptibility to CuNPs. The other two isolates, S.73 and S.76, showed inhibition down to15.6 µg/ml, but no effect was observed at lower concentrations.

Also shown that the antibacterial activity of CuNPs can be influenced by factors such as upon various factors, including the nanoparticles' shape and size, the bacterial strains tested, the inoculum size and the presence of capping agents. The most-

Table 1. Zone of inhibition diameters for CuNP tested at incremental concentrations against *S. aureus*.

Concentration (µg / ml)	Median (Interquartile Range) of zone of inhibition (mm)
1000	27 (21.15 - 27.7)[a]
500	20.1 (18.15 - 20.25)[ae]
250	19 (18 - 19.8)[ac]
125	18.8 (17.9 - 19.5)[ac]
62.5	15.7 (15.3 - 15.9)[bce]
31.25	14.3 (14.2 - 15)[bce]
15.6	11.9 (11.8 - 14.75)[bc]
7.8	0 (0 - 12.85)[b]
3.9	0 (0 - 0)[b]

Data presented as median and Interquartile range. Medians with similar superscript lowercase letter have non-significant differences determined by Kruskal-Wallis test followed by Dunn's multiple comparisons test Error bars represent median and interquartile range. Asterisks denote statistical significance: $p < 0.05$ (*), $p < 0.01$ (**), $p < 0.001$ (***), and $p < 0.0001$ (****), as determined by the Kruskal–Wallis test followed by Dunn's multiple comparisons test.

Table 2. The Minimum Inhibitory Concentrations (MIC) of CNPs against *S. aureus* using resazurin based method.

Bacterial isolate	MIC of CuNPs (µg/ml)
S. aureus 73	7.8
S. aureus 75	15.6
S. aureus 76	7.8

reported mechanism for CuNPs is based on the generation reactive oxygen species (ROS). Cu NPs also enhance the cellular ROS level dramatically that influences lipid peroxidation, oxidation protein and destruction of DNA and kills the microorganism cells [46]. The ROS contain radical compounds such as hydroxyl (-OH), superoxide radical (O^{2-}), singlet oxygen ($1O_2$) and hydrogen peroxide (H_2O_2) which bacteria destroy, In addition to oxidative stress as pervious study report. This result agreed with pervious study reported by [47] the zone diameter increased as the CuNps concentration increased. The most effective stock solution in gram positive bacterial strains is 1000 µg / ml. Diameters of inhibition zones are seen at this concentration; 16.5 mm in *S. aureus*. The schematic diagram of the biosynthesis of aqueous extract and antibacterial activity CuNPs using *A. ampeloprasum* is shown in Fig. 13.

Minimum Inhibitory Concentration of CuNPs

The lowest MIC of CuNPs for two isolates against *S. aureus* was determined for each isolate Table 2.

The concentrations of CuNP regarded as MIC, are those who have no detectable growth is observed. Higher concentrations of CuNP (1000 µg/ml) had a strong effect on cell viability of bacteria for all isolates in in Muller Hinton broth, while lowest concentrations of CuNP regarded as MIC for *S. aureus 73, 76 and 75* isolates was 7.8, 15.6 and 7.8 g/ml respectively, the result is shown in Fig. 14. CuNP are positively charged, while the both Gram-positive surface are negatively charged. Therefore, CuNP can be on the cell membrane combined with negatively charged areas, to the potential difference reduce and depolarization cause. It will cause leakage or even rupture for membrane and bacterial death eventually [48]. Many studies have

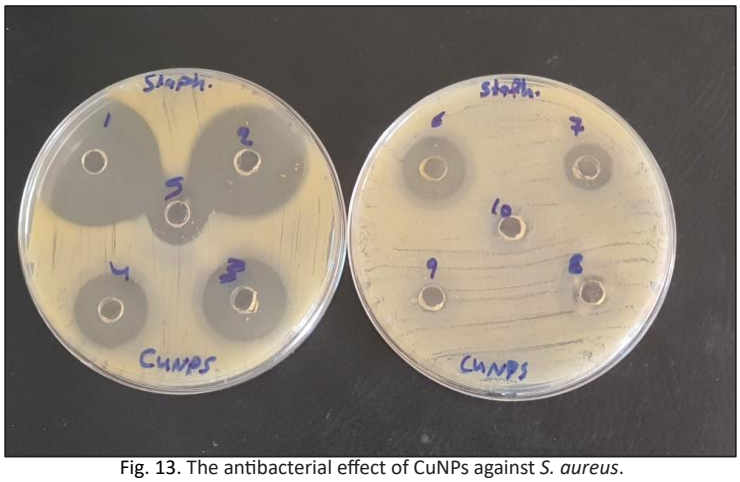

Fig. 13. The antibacterial effect of CuNPs against *S. aureus*.

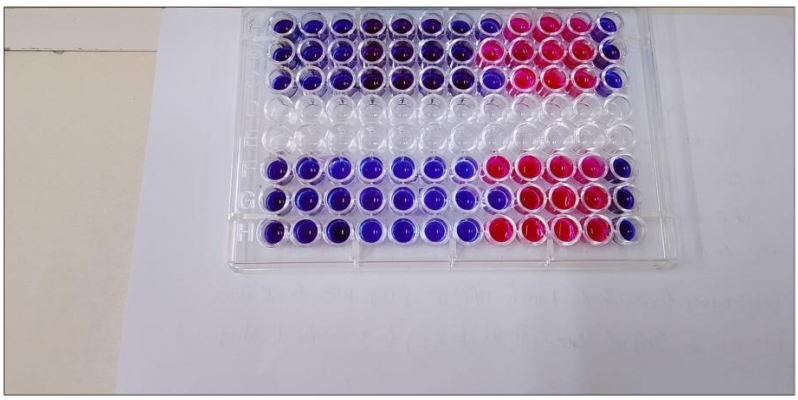

Fig. 14. The Minimum Inhibitory concentrations of the CuNPs against *S. aureus*.

shown that the copper exposure is a direct target to cell membrane [49]. However, bactericidal effect of CuNP on Gram-positive bacteria is strong, which may be due to the cell wall structure of these two classes difference. The result of the search is not in the line with previous studies on the minimum inhibitory concentration of CuNPs.

CONCLUSION

In this study, CuNPs were produced successfully from *A. ampeloprasum* using a simple, direct, low-cost, high yield and environmentally friendly approach. CuNPs showed an outstanding antimicrobial activity when tested against several Multi-resistant bacterial isolates, which have an alarming situation create that has encouraged the new therapies development for infections and diseases.

CONFLICT OF INTEREST

The authors declare that there is no conflict of interests regarding the publication of this manuscript.

REFERENCES

1. Daniel M-C, Astruc D. Gold Nanoparticles: Assembly, Supramolecular Chemistry, Quantum-Size-Related Properties, and Applications toward Biology, Catalysis, and Nanotechnology. Chem Rev. 2003;104(1):293-346.
2. Tian Y, Tatsuma T. Plasmon-induced photoelectrochemistry at metal nanoparticles supported on nanoporous TiO_2. Chem Commun. 2004(16):1810.
3. Kalidindi SB, Sanyal U, Jagirdar BR. Nanostructured Cu and Cu@Cu2O core shell catalysts for hydrogen generation from ammonia–borane. Physical Chemistry Chemical Physics. 2008;10(38):5870.
4. Grzelczak M, Pérez-Juste J, Mulvaney P, Liz-Marzán LM. Shape control in gold nanoparticle synthesis. Chem Soc Rev. 2008;37(9):1783.
5. Antibacterial Activity of Copper Nanoparticles Synthesized by Bambusa arundinacea Leaves Extract. Biointerface Research in Applied Chemistry. 2021;12(1):1230-1236.
6. Rajeshkumar S, Menon S, Venkat Kumar S, Tambuwala MM, Bakshi HA, Mehta M, et al. Antibacterial and antioxidant potential of biosynthesized copper nanoparticles mediated through Cissus arnotiana plant extract. J Photochem Photobiol B: Biol. 2019;197:111531.
7. Asghar MA, Asghar MA. RETRACTED: Green synthesized and characterized copper nanoparticles using various new plants extracts aggravate microbial cell membrane damage after interaction with lipopolysaccharide. Int J Biol Macromol. 2020;160:1168-1176.
8. Cucci LM, Satriano C, Marzo T, La Mendola D. Angiogenin and Copper Crossing in Wound Healing. Int J Mol Sci. 2021;22(19):10704.
9. Wang L-j, Ni X-h, Zhang F, Peng Z, Yu F-x, Zhang L-b, et al. Osteoblast Response to Copper-Doped Microporous Coatings on Titanium for Improved Bone Integration. Nanoscale Research Letters. 2021;16(1).
10. Alizadeh S, Seyedalipour B, Shafieyan S, Kheime A, Mohammadi P, Aghdami N. Copper nanoparticles promote rapid wound healing in acute full thickness defect via acceleration of skin cell migration, proliferation, and neovascularization. Biochemical and Biophysical Research Communications. 2019;517(4):684-690.
11. Dollwet HHA, Sorenson JRJ. Roles of copper in bone maintenance and healing. Biol Trace Elem Res. 1988;18(1):39-48.
12. Sen CK, Khanna S, Venojarvi M, Trikha P, Ellison EC, Hunt TK, et al. Copper-induced vascular endothelial growth factor expression and wound healing. American Journal of Physiology-Heart and Circulatory Physiology. 2002;282(5):H1821-H1827.
13. Habibovic P, Barralet JE. Bioinorganics and biomaterials: Bone repair. Acta Biomater. 2011;7(8):3013-3026.
14. Bondarenko O, Juganson K, Ivask A, Kasemets K, Mortimer M, Kahru A. Toxicity of Ag, CuO and ZnO nanoparticles to selected environmentally relevant test organisms and mammalian cells in vitro: a critical review. Arch Toxicol. 2013;87(7):1181-1200.
15. El Said GAD, El-Shabrawy M, El-Sageer, El-Jakee J. Phage Typing of Staphylococcus Aureus Isolated from Dairy Cows in Egypt. Veterinary Medical Journal (Giza). 1996;44(1):85-93.
16. Rahimzadeh Torabi L, Sadat Naghavi N, Doudi M, Monajemi R. Efficacious antibacterial potency of novel bacteriophages against ESBL-producing Klebsiella pneumoniae isolated from burn wound infections. Iranian Journal of Microbiology. 2021.
17. Zhao N, Cheng D, Jian Y, Liu Y, Liu J, Huang Q, et al. Molecular characteristics of Staphylococcus aureus isolates colonizing human nares and skin. Medicine in Microecology. 2021;7:100031.
18. Alshomrani MK, Alharbi AA, Alshehri AA, Arshad M, Dolgum S. Isolation of Staphylococcus aureus Urinary Tract Infections at a Community-Based Healthcare Center in Riyadh. Cureus. 2023.
19. de Sousa T, Hébraud M, Alves O, Costa E, Maltez L, Pereira JE, et al. Study of Antimicrobial Resistance, Biofilm Formation, and Motility of Pseudomonas aeruginosa Derived from Urine Samples. Microorganisms. 2023;11(5):1345.
20. Delgado E. Salmonella spp. antibiotic susceptibility testing by the Kirby-Bauer disk diffusion method v1. Springer Science and Business Media LLC; 2020.
21. F Hussein E. Detection and Antibiotic Susceptibility Patterns of Staphylococcus aureus, Streptococcus pyogenes and Streptococcus spp. Isolated from Sputum of Patients with Respiratory Tract Infections. Journal of Communicable Diseases. 2024;56(01):50-56.
22. An Overview of the Clinical and Laboratory Standards Institute (CLSI) and Its Impact on Antimicrobial Susceptibility Tests. Antimicrobial Susceptibility Testing Protocols: CRC Press; 2007. p. 15-20.
23. Velsankar K, R.M AK, R P, V M, Sudhahar S. Green synthesis of CuO nanoparticles via Allium sativum extract and its characterizations on antimicrobial, antioxidant, antilarvicidal activities. Journal of Environmental Chemical Engineering. 2020;8(5):104123.
24. Abed SM, Mahmood YS, Waheed IF, Alwan AM. Antibacterial Activity of Green Synthesized Copper Oxide Nanoparticles. Iraqi Journal of Science. 2021:3372-3383.
25. Some Applications of Uv and Vis Spectrophotometry. Studies in Analytical Chemistry: Elsevier; 1989. p. 260-303.
26. Kamnev AA, Dyatlova YA, Kenzhegulov OA, Vladimirova AA, Mamchenkova PV, Tugarova AV. Fourier Transform Infrared

(FTIR) Spectroscopic Analyses of Microbiological Samples and Biogenic Selenium Nanoparticles of Microbial Origin: Sample Preparation Effects. Molecules. 2021;26(4):1146.
27. Prabu P, Losetty V. Green synthesis of copper oxide nanoparticles using Macroptilium Lathyroides (L) leaf extract and their spectroscopic characterization, biological activity and photocatalytic dye degradation study. J Mol Struct. 2024;1301:137404.
28. Vladár AE, Hodoroaba V-D. Characterization of nanoparticles by scanning electron microscopy. Characterization of Nanoparticles: Elsevier; 2020. p. 7-27.
29. Bin Mobarak M, Hossain MS, Chowdhury F, Ahmed S. Synthesis and characterization of CuO nanoparticles utilizing waste fish scale and exploitation of XRD peak profile analysis for approximating the structural parameters. Arabian Journal of Chemistry. 2022;15(10):104117.
30. Feyzioglu GC, Tornuk F. Development of chitosan nanoparticles loaded with summer savory (Satureja hortensis L.) essential oil for antimicrobial and antioxidant delivery applications. LWT. 2016;70:104-110.
31. Stetefeld J, McKenna SA, Patel TR. Dynamic light scattering: a practical guide and applications in biomedical sciences. Biophys Rev. 2016;8(4):409-427.
32. Shiravand S, Azarbani F. Phytosynthesis, characterization, antibacterial and cytotoxic effects of copper nanoparticles. Green Chemistry Letters and Reviews. 2017;10(4):241-249.
33. Akshaya T, Aravind M, Manoj Kumar S, Divya B. Evaluation of In-Vitro Antibacterial Activity Against Gram-Negative Bacteria Using Silver Nanoparticles Synthesized from Dypsis lutescens LEAF EXTRACT. Journal of the Chilean Chemical Society. 2022;67(2):5477-5483.
34. Mirzaei R, Alikhani MY, Arciola CR, Sedighi I, Irajian G, Jamasbi E, et al. Highly Synergistic Effects of Melittin With Vancomycin and Rifampin Against Vancomycin and Rifampin Resistant Staphylococcus epidermidis. Front Microbiol. 2022;13.
35. Peng Q, Tang X, Dong W, Sun N, Yuan W. A Review of Biofilm Formation of Staphylococcus aureus and Its Regulation Mechanism. Antibiotics. 2022;12(1):12.
36. Ghayyib AA, Ahmed IA, Ahmed HK. Isolation and Characterization of Staphylococcus Phage Rih21 and Evaluation of its Antibacterial Activity against Methicillin-resistant Staphylococcus aureus Clinical Isolates. MDPI AG; 2022.
37. Prasanna S, Dharanidevi S, Kumar Das N, Raj S. Prevalence, Phenotypic Characterization and Antibiotic Susceptibility of Non-Fermentative Gram Negative Bacilli Isolates at a Tertiary Care Centre. International Journal of Current Microbiology and Applied Sciences. 2016;5(11):442-454.
38. Naimi HM, Rasekh H, Noori AZ, Bahaduri MA. Determination of antimicrobial susceptibility patterns in Staphylococcus aureus strains recovered from patients at two main health facilities in Kabul, Afghanistan. BMC Infect Dis. 2017;17(1).
39. Study on the prevalence of methicillin-resistant Staphylococcus aureus infection, antibiotic resistance pattern, biofilms genes, and antibiotic resistance genes from clinical samples. Archives of Razi Institute. 2023:923-928.
40. Kausar H, Mehmood A, Khan RT, Ahmad KS, Hussain S, Nawaz F, et al. Green synthesis and characterization of copper nanoparticles for investigating their effect on germination and growth of wheat. PLoS One. 2022;17(6):e0269987.
41. Venugopalan R, Pitchai S, Devarayan K, Swaminathan VC. Biogenic synthesis of copper nanoparticles using Borreria hispida (Linn.) extract and its antioxidant activity. Materials Today: Proceedings. 2020;33:4023-4025.
42. Rojas B, Soto N, Villalba M, Bello-Toledo H, Meléndrez-Castro M, Sánchez-Sanhueza G. Antibacterial Activity of Copper Nanoparticles (CuNPs) against a Resistant Calcium Hydroxide Multispecies Endodontic Biofilm. Nanomaterials. 2021;11(9):2254.
43. Betancourt-Galindo R, Reyes-Rodriguez PY, Puente-Urbina BA, Avila-Orta CA, Rodríguez-Fernández OS, Cadenas-Pliego G, et al. Synthesis of Copper Nanoparticles by Thermal Decomposition and Their Antimicrobial Properties. Journal of Nanomaterials. 2014;2014(1).
44. Romi ZM, Ahmed ME. The Influence of Biologically Synthesized Copper Nanoparticles on the Biofilm Produced by Staphylococcus haemolyticus 1solated from Seminal Fluid. Iraqi Journal of Science. 2024:1948-1968.
45. Gour A, Jain NK. Advances in green synthesis of nanoparticles. Artificial Cells, Nanomedicine, and Biotechnology. 2019;47(1):844-851.
46. Zhang B, Slavkovic S, Qiu Y, Peng C, Chen JIL. Nickel coating on plasmonic copper nanoparticles lowers cytotoxicity and enables colorimetric pH readout for antibacterial wound dressing application. Nanoscale Advances. 2024;6(17):4462-4469.
47. Mitra D, Kang E-T, Neoh KG. Antimicrobial Copper-Based Materials and Coatings: Potential Multifaceted Biomedical Applications. ACS Applied Materials and Interfaces. 2019;12(19):21159-21182.
48. Başar Y, Yiğit A, Karacalı Tunç A, Sarıtaş BM. Lavandula Stoechas extract; Synthesis of Silver Nanoparticles (Nature-Friendly Green Synthesis Method), Characterization, Antimicrobial Activity and In Silico Molecular Docking Study. Current Perspectives on Medicinal and Aromatic Plants (CUPMAP). 2024.
49. Santo CEr, Lam EW, Elowsky CG, Quaranta D, Domaille DW, Chang CJ, et al. Bacterial Killing by Dry Metallic Copper Surfaces. Applied and Environmental Microbiology. 2011;77(3):794-802.
50. Warnes SL, Caves V, Keevil CW. Mechanism of copper surface toxicity in Escherichia coli O157:H7 and Salmonella involves immediate membrane depolarization followed by slower rate of DNA destruction which differs from that observed for Gram-positive bacteria. Environ Microbiol. 2011;14(7):1730-1743.